PHYSICAL REVIEW B **77**, 060505(R) (2008)

Superconductivity phase diagrams for the electron-doped cuprates $R_{2-x}Ce_xCuO_4$ (R=La, Pr, Nd, Sm, and Eu)

Y. Krockenberger,[1,2,*] J. Kurian,[1,2] A. Winkler,[1,2] A. Tsukada,[2,3] M. Naito,[2,3] and L. Alff[1,†]
[1]*Institute for Materials Science, TU Darmstadt, Petersenstrasse 23, 64287 Darmstadt, Germany*
[2]*NTT Basic Research Laboratories, 3-1 Wakamiya, Atsugi-shi, Kanagawa 243-0198, Japan*
[3]*Department of Applied Physics, Tokyo University of Agriculture and Technology (TUAT), Tokyo, Japan*
(Received 9 November 2007; revised manuscript received 11 December 2007; published 27 February 2008)

The superconductivity phase diagrams of electron-doped cuprates of the form $R_{2-x}Ce_xCuO_4$ (with R=La, Pr, Nd, Sm, and Eu) have been determined for cerium compositions $0<x<0.36$ in a consistent series of epitaxial thin films grown by reactive molecular beam epitaxy. The use of epitaxial thin films allows the growth of materials away from thermodynamical equilibrium expanding the accessible phase space beyond the availability of bulk material. The superconducting phase space systematically increases with the rare-earth ionic size. The doping concentration where the maximal transition temperature occurs in $La_{2-x}Ce_xCuO_4$ is considerably shifted to lower doping ($x\sim0.09$) compared to $La_{2-x}Sr_xCuO_4$ ($x\sim0.15$). At the same time, the width of the superconducting region is broadened.

DOI: 10.1103/PhysRevB.77.060505 PACS number(s): 74.25.Dw, 74.72.Dn, 74.78.Bz

The phase diagram of cuprate superconductors is a key ingredient to understand the still unresolved mechanism of high-temperature superconductivity. A particular interesting question is the comparison of the phase diagrams for hole and electron doping.[1] A theory of high-temperature superconductivity has to explain the occurring differences and similarities when a copper-oxide plane is doped by holes or electrons. While for the hole-doped case there is already an overwhelming amount of experimental data available, the electron-doped side of the phase diagram still needs *experimental clarification*. Electron-doped cuprates are widely identified with the two materials $Nd_{2-x}Ce_xCuO_4$ (Ref. 2) and $Pr_{2-x}Ce_xCuO_4$. In contrast to the hole-doped cuprates where in compounds of the form $R_{2-x}Sr_xCuO_4$ only for R=La superconductivity shows up, for the electron-doped side of the phase diagram a whole family of superconductors of the form $R_{2-x}Ce_xCuO_4$ (R=La, Pr, Nd, Sm, and Eu) exists. It is solely due to historical reasons that most investigations of electron-doped cuprates have been made for $Nd_{2-x}Ce_xCuO_4$ and $Pr_{2-x}Ce_xCuO_4$. These two materials have an almost identical ionic radius and also show, therefore, also a very similar phase diagram. This has led to the common belief that these properties of a *specific* electron-doping phase diagram (in particular a narrow superconducting region) is intrinsic to electron-doped cuprates *in general*. In addition, for $Nd_{2-x}Ce_xCuO_4$ (and to a lesser extent for $Pr_{2-x}Ce_xCuO_4$) the magnetism of Nd^{3+} (and Pr^{3+}) masks in some experiments the intrinsic properties of the superconductor such as the temperature dependence of the London penetration depth.[3] Moreover, the difficulties in bulk sample preparation makes the determination of exact phase diagrams a much debated topic.[4–6] Using reactive molecular beam epitaxy (MBE)[7] and pulsed laser deposition (PLD)[8] recently superconducting epitaxial thin films of $La_{2-x}Ce_xCuO_4$ have been successfully grown. For bulk material up to now only the mixed compound $LaPr_{1-x}Ce_xCuO_4$ could be synthesized,[9,10] and is now intensively studied.[11–13] Here we present a consistent and detailed study of the complete electron-doped family $R_{2-x}Ce_xCuO_4$ (with R=La, Pr, Nd, Sm, and Eu) based on MBE-grown epitaxial thin films. The key results are that the width of the superconducting phase space increases systematically with the ionic size of the rare-earth element L, and that the doping level of maximal superconductivity with highest critical temperature T_C is not fixed (to $x\approx0.15$), but shifts to significantly lower doping. We conclude that the most meaningful comparison of the superconductivity phase diagrams of hole- and electron-doped cuprates that can be done given this material's situation, should be made using La-based cuprates. However, one still has to keep in mind that $La_{2-x}Sr_xCuO_4$ has the so-called T structure (K_2NiF_4 structure) containing apical oxygen, while $La_{2-x}Ce_xCuO_4$ with $x\gtrsim0.05$ has the so-called T' structure (Nd_2CuO_4 structure) where the Cu ion is only fourfold coordinated, i.e., the apical oxygen ions are missing. The structural difference translates into different ionic radii of the Cu^{2+} ions: 0.73 Å in the T structure and 0.57 Å in the T' structure (reduction of more than 20%). It is still one of the most exciting future challenges in high-T_C research to find a system where a *direct* comparison of hole and electron doping can be made in a wide range of doping. All our films were grown by reactive MBE using simultaneous electron-beam evaporation from elemental sources on (001) $SrTiO_3$ substrates. The stoichiometry was controlled by electron-impact emission spectroscopy (EIES). A typical growth scenario of electron-doped superconducting thin films is shown in Fig. 1. Films are grown at a substrate temperature of about 700 °C in an ozone pressure of about 2×10^{-6} Torr. During growth the sample has to be in the region of divalent copper (correspondingly the rare-earth elements are 3+ and Ce 4+). Growth rates are approximately 3 Å/s leading to homogeneous and precipitate free epitaxial thin films. It is well known that the oxygen contents of electron-doped cuprates is a crucial and so far not fully understood issue.[14–17] We have adopted a consistent sample treatment in order to exclude as far as possible different oxygen content in our samples: all samples were annealed in vacuum at temperatures close to the stability line of each compound. The stability lines shown in Fig. 1 have been determined experimentally by observing

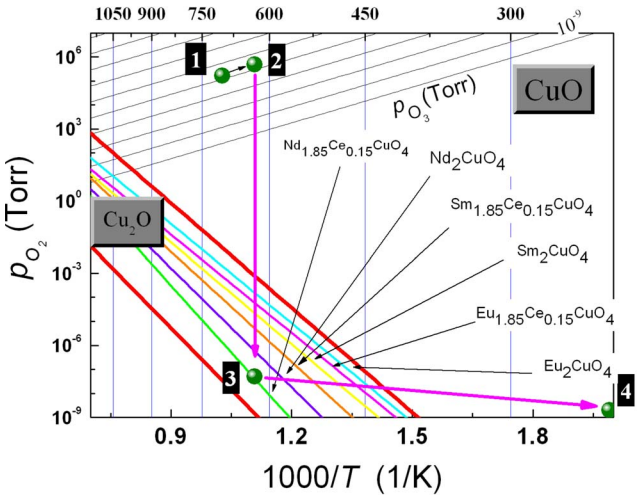

FIG. 1. (Color online) Typical thermodynamic phase stability diagram for electron-doped cuprates. Stability lines for CuO and Cu_2O have been calculated using the commercially available program MALT®. Additionally, the equilibria oxidizing potential lines for ozone and oxygen are calculated. The numbered points describe a typical growth of the thin film. The border lines for the different copper valencies are thick red colored. Between them, all experimentally established stability lines for the T'-structure compounds are lying. Points 1 and 2 represent the growth followed by annealing in vacuum (point 3) and afterwards cooled down to point 4.

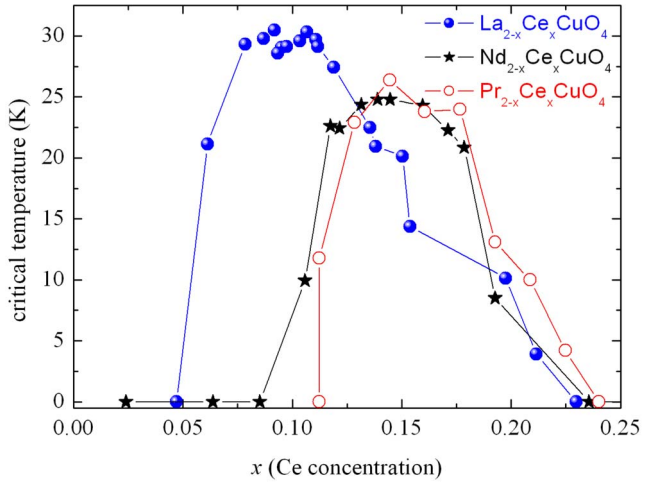

FIG. 2. (Color online) Superconductivity phase diagrams of $La_{2-x}Ce_xCuO_4$, $Nd_{2-x}Ce_xCuO_4$, and $Pr_{2-x}Ce_xCuO_4$.

in real time the reflection high-energy electron diffraction (RHEED) signal which indicates starting decomposition. This procedure adopted in the present investigation enables the comprehensive removal of excess oxygen without any measurable decomposition due to too strong reduction. In the case of bulk material synthesis, the reduction process may either lead to noncomplete removal of excess oxygen, or to partial decomposition of the material.[17,18] Another important issue for electron-doped cuprates is the presence of disorder that can affect T_C seriously. Taking room-temperature resistivity as a measure of disorder, for our study a correlation between disorder and ionic radii of the lanthanide ions can be excluded, since all compounds $R_{2-x}Ce_xCuO_4$ (with R =La, Pr, Nd, and Sm) have at optimal doping very similar resistivity, except for Eu where the possible role of disorder cannot be ruled out. For all samples Ce-doping reduces linearly the c-axis parameter because the ionic radius of Ce^{4+} is 0.97 Å, which is smaller than the radius of the rare-earth elements. The typical thickness of the films in the present study was ~1000 Å.

$La_{2-x}Ce_xCuO_4$. Of course, it would be a breakthrough in the research on electron-doped cuprates to make available bulk material of $La_{2-x}Ce_xCuO_4$ in the Nd_2CuO_4 structure. For thin film growth in ultrahigh vacuum far from thermodynamic equilibrium, epitaxial growth of T' $La_{2-x}Ce_xCuO_4$ is possible at a substrate temperature of 700 °C and in a partial ozone pressure of 2×10^{-6} Torr. As has been shown before, the structural phase transition into the T phase occurs for $x\lesssim0.05$.[7] However, a further reduction of growth temperature by 100 °C allows the growth of T'-phase $La_{2-x}Ce_xCuO_4$ even down to $x=0$ but at the cost of crystalline quality. It is even possible to stabilize the T' phase with improved crystallinity by substitution of smaller trivalent ions such as Tb, Y, etc.[19] In Fig. 2 we show the obtained phase diagram for $La_{2-x}Ce_xCuO_4$. The two major observations are (i) the strongly broadened superconductivity region ranging from $x\approx0.05$ to $x\approx0.22$, and (ii) the maximal T_C of 32 K occurring at $x\approx0.09$. Sawa *et al.*[8] claim a complete shift (i.e., no broadening) of the superconductivity region based on thin films grown by PLD if samples have high dopant homogeneity. However, the broader superconducting region as confirmed in this paper is clearly not due to any inhomogeneities of the samples. First, the sample size is too small (3 mm by 5 mm) to expect compositional inhomogeneities in the given MBE setup. For example, three different samples attached to the heater and grown in the same run give exactly the same T_C. Second, the resistivity values of the MBE grown films are well below those of the PLD thin films.[7,8] Third, the critical temperature in the MBE grown thin films (see Fig. 2) is higher than compared to PLD samples.[8] Fourth, the superconducting transition width in resistivity and magnetometry is even sharper for higher doping where the extended superconducting region is observed in this study. The room-temperature resistivity values of $La_{2-x}Ce_xCuO_4$ films lies between 0.22–2.0 mΩ cm for optimal and undoped samples, respectively.

$Pr_{2-x}Ce_xCuO_4$ and $Nd_{2-x}Ce_xCuO_4$. The corresponding superconductivity phase diagrams of MBE grown films are included in Fig. 2 for a direct comparison. The superconductivity region extends from $x\approx0.10$ to $x\approx0.24$, and the maximal T_C of 26 K occurs for $x\approx0.145$. Note also, that UHV annealing times and growth temperatures differ slightly for different x. In this study we have always used the parameters yielding the highest T_C for a given doping concentration x. The simple trend is that for the highest crystallinity [as indicated in a standard x-ray diffraction pattern by the intensity of the (006) reflection of the epitaxial thin film], also the highest T_C is obtained. The phase diagram based on thin film data fully agrees with the huge amount of published data for bulk material of $Pr_{2-x}Ce_xCuO_4$ and $Nd_{2-x}Ce_xCuO_4$. The room temperature resistivity of optimal-doped samples

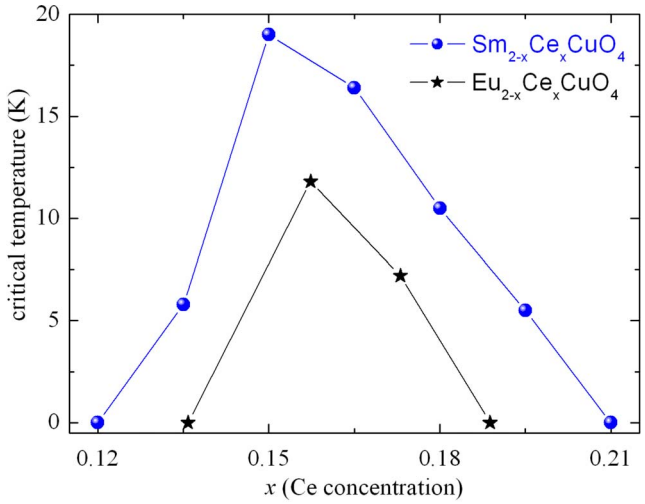

FIG. 3. (Color online) Superconductivity phase diagrams of $Sm_{2-x}Ce_xCuO_4$ and $Eu_{2-x}Ce_xCuO_4$.

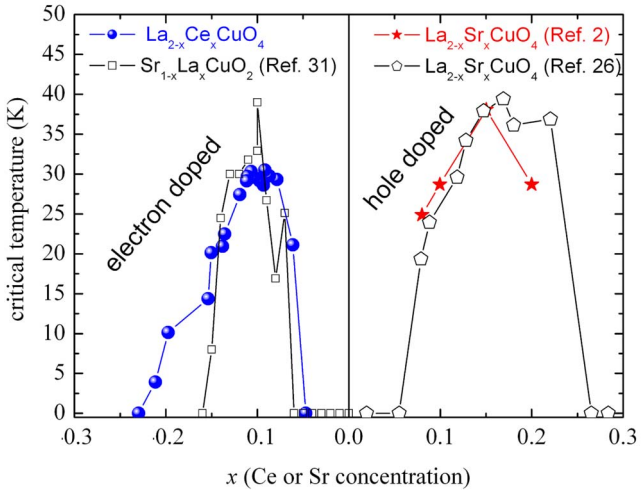

FIG. 4. (Color online) Direct comparison of La-based cuprates with respect to electron and hole doping: Superconductivity phase diagrams of $La_{2-x}Ce_xCuO_4$ (thin film data) and $La_{2-x}Sr_xCuO_4$ (bulk data[2,25]).

of $Pr_{2-x}Ce_xCuO_4$ and $Nd_{2-x}Ce_xCuO_4$ films were 0.26 and 0.23 mΩ cm, respectively, whereas for undoped samples the respective values were 5.6 and 8.9 mΩ cm.

$Sm_{2-x}Ce_xCuO_4$. The ionic radius of eightfold coordinated Sm^{3+} is 1.079 Å. From Fig. 3 one sees that the maximal T_C of 19 K is obtained for $x=0.150$, consistent with earlier bulk data.[20] The room-temperature and low-temperature resistivity values show also minima around $x\approx 0.15$. The resistivity range at room temperature for $Sm_{2-x}Ce_xCuO_4$ thin films lies between 0.2 mΩ cm and 100 mΩ cm for optimal-doped and undoped samples, respectively. Superconductivity occurs in the range of approximately $x\approx 0.13$ to $x\approx 0.20$. Bulk superconductivity in $Sm_{2-x}Ce_xCuO_4$ has been reported by several authors.[21,22]

$Eu_{2-x}Ce_xCuO_4$. The right-hand side neighbor of Sm in the periodic table is Eu. Shortly after electron-doped cuprates had been discovered, Markert *et al.*[23] reported on superconductivity in $Eu_{2-x}Ce_xCuO_4$, however, so far no results on thin films have been reported. The ionic radius of eightfold coordinated Eu^{3+} is 1.066 Å. The superconducting region is very limited between $0.14<x<0.19$. Maximal T_C of 12 K occurs at $x=0.16$. The phase diagram is shown in Fig. 3. The resistivity range at room temperature for $Eu_{2-x}Ce_xCuO_4$ thin films lies between 0.6 mΩ cm and 140 mΩ cm for optimal-doped and undoped samples, respectively.

The combined results of our thin-film study of $R_{2-x}Ce_xCuO_4$ (with R=La, Pr, Nd, Sm, and Eu) show that the superconductivity phase diagrams depend systematically on the rare-earth ionic radius of the compound. The $Gd_{2-x}Ce_xCuO_4$ ($x=0$ to 0.21) thin films grown by reactive MBE did not show superconductivity in the whole Ce concentration range studied. Superconductivity can only be observed above a threshold ionic size of about 1.053 Å of Gd^{3+} (or tolerance factor >0.83).[24] The superconducting phase region expands significantly with L^{3+} ionic radii, i.e., for R =La the superconducting region spans from $x=0.05$ to $x=0.22$, whereas for R=Eu, it is from $x=0.14$ to $x=0.19$. Correspondingly, it is also observed that the maximal T_c increases with ionic radii (for R=La−31 K and R=Eu−12 K) and it occurs at considerably lower doping (i.e., for R=La at $x=0.09$, whereas R=Eu at $x=0.16$). In other words, with increasing ionic radius, not only the superconducting phase region expands, but also the maximal T_C increases, and the doping level where it is observed is shifted towards lower doping. The end point is set by $La_{2-x}Ce_xCuO_4$, which hits at low doping ($x\lesssim 0.05$) the instability line where the structural transition from T' into T structure occurs. The breakdown of superconductivity in $La_{2-x}Ce_xCuO_4$ around $x\approx 0.05$ therefore is clearly due to this structural phase transition. As underdoped samples below $x\approx 0.05$ are not systematically available, the experimental evaluation of the phase competition between superconductivity and antiferromagnetism is elusive. The important issue is clearly how to compare electron- and hole-doped compounds experimentally. Based on our results, it is suggestive that this comparison should be made in the system $La_{2-x}X_xCuO_4$ with X=Sr and Ce. The caveat here is that one is still dealing with a different crystal structure. The key result of this paper is summarized in Fig. 4. Here, we compare directly $La_{2-x}Ce_xCuO_4$ and $La_{2-x}Sr_xCuO_4$. The $La_{2-x}Sr_xCuO_4$ data are taken from literature and have been obtained from bulk materials (i.e., no effects of substrate strain are considered that can increase T_C). The comparison of hole- and electron-doped cuprates made in Fig. 4 is the most direct possible with available data. The width of the superconducting phase region is very similar for hole and electron doping. The electron-doped side of the phase diagram even extends to slightly lower doping. The absolute value of T_C is about 10 K (or 33%) higher in the hole-doped case. Surprisingly, the doping where the maximal T_C occurs at the electron-doped side is shifted to below $x=0.1$ for $La_{2-x}Ce_xCuO_4$, which is a reduction by about one third compared to hole doping. There is no such thing as a distinguished intrinsic doping value of about $x\approx 0.15$ where maximal superconductivity occurs in cuprate high-temperature superconductors. In most Hubbard model calculations (see, for example, recent variational cluster perturbation theory in the $t-t'-t''-U$ Hubbard model[26] and also

recent quantum Monte Carlo simulations[27]), the phase competition between *d*-wave superconductivity and antiferromagnetism comes out similar to experimentally observed for the unspecific phase diagram of $Nd_{2-x}Ce_xCuO_4$ and $Pr_{2-x}Ce_xCuO_4$, i.e., for electron doping the antiferromagnetic phase persists to higher doping before superconductivity sets in, and the superconducting region is narrower compared to the hole-doping case. With respect to the superconducting part of the phase diagram, our experimental results here show that these properties are not intrinsic or generally valid for electron-doped cuprates. From our thin film experiments, we cannot establish the antiferromagnetic region of the phase diagram. It is possible that in a certain doping range both order parameters coexist.[28,29] It remains a theoretical task to understand the presented superconductivity phase diagrams of electron-doped cuprates. Note that the phase diagram of the electron-doped infinite layer compound $Sr_{1-x}La_xCuO_2$ where copper is fourfold coordinated, as is the case in the T' structure, shows maximal superconductivity also around $x \approx 0.1$.[30]

In summary, we have shown by a consistent study of MBE-grown cuprate thin films that the superconductivity phase diagrams of the electron-doped cuprates depend strongly on the rare-earth ionic radius. The most suitable compound for a comparison of hole and electron doped cuprates so far is $La_{2-x}Ce_xCuO_4$. The extended superconductivity range and the occurrence of maximal T_C at considerably reduced doping indicates even slightly higher superconductivity phase stability for the electron-doped side of the phase diagram.

The authors acknowledge support by the DFG (Contract No. FOR 538) and fruitful discussions with Ch. Bernhard, D. Manske, P. Yordanov, and H. Yamamoto.

*yoshiharu.krockenberger@aist.go.jp
†alff@oxide.tu-darmstadt.de

[1] Y. Tokura, H. Takagi, and S. Uchida, Nature (London) **337**, 345 (1989).
[2] G. M. Luke *et al.*, Phys. Rev. B **42**, 7981 (1990).
[3] L. Alff, S. Meyer, S. Kleefisch, U. Schoop, A. Marx, H. Sato, M. Naito, and R. Gross, Phys. Rev. Lett. **83**, 2644 (1999).
[4] H. J. Kang, P. Dai, J. W. Lynn, M. Matsuura, J. R. Thompson, S.-C. Zhang, D. N. Argyriou, Y. Onose, and Y. Tokura, Nature (London) **423**, 522 (2003).
[5] P. K. Mang, S. Larochelle, and M. Greven, Nature (London) **426**, 139 (2003).
[6] H. J. Kang, Pengcheng Dai, J. W. Lynn, M. Matsuura, J. R. Thompson, Shou-Cheng Zhang, D. N. Argyriou, Y. Onose, and Y. Tokura, Nature (London) **426**, 140 (2003).
[7] M. Naito and M. Hepp, Jpn. J. Appl. Phys., Part 2 **39**, L485 (2000).
[8] A. Sawa, M. Kawasaki, H. Takagi, and Y. Tokura, Phys. Rev. B **66**, 014531 (2002).
[9] T. Uefuji, K. Kurahashi, M. Fujita, M. Matsuda, and K. Yamada, Physica C **378-381**, 273 (2002).
[10] M. Fujita, T. Kubo, S. Kuroshima, T. Uefuji, K. Kawashima, K. Yamada, I. Watanabe, and K. Nagamine, Phys. Rev. B **67**, 014514 (2003).
[11] H. Matsui, K. Terashima, T. Sato, T. Takahashi, M. Fujita, and K. Yamada, Phys. Rev. Lett. **95**, 017003 (2005).
[12] S. D. Wilson, Shiliang Li, Hyungje Woo, Pengcheng Dai, H. A. Mook, C. D. Frost, S. Komiya, and Y. Ando, Phys. Rev. Lett. **96**, 157001 (2006).
[13] S. D. Wilson, Pengcheng Dai, Shiliang Li, Songxue Chi, H. J. Kang, and J. W. Lynn, Nature (London) **442**, 59 (2006).
[14] P. Richard, G. Riou, I. Hetel, S. Jandl, M. Poirier, and P. Fournier, Phys. Rev. B **70**, 064513 (2004).
[15] J. S. Higgins, Y. Dagan, M. C. Barr, B. D. Weaver, and R. L. Greene, Phys. Rev. B **73**, 104510 (2006).
[16] W. Yu, B. Liang, P. Li, S. Fujino, T. Murakami, I. Takeuchi, and R. L. Greene, Phys. Rev. B **75**, 020503(R) (2007).
[17] H. J. Kang, P. Dai, B. J. Campbell, P. J. Chupas, S. Rosenkranz, P. L. Lee, Q. Huang, S. Li, S. Komiya, and Y. Ando, Nat. Mater. **6**, 224 (2007).
[18] J. Hauck, K. Bickmann, and K. Mika, Supercond. Sci. Technol. **11**, 63 (1998).
[19] A. Tsukada, Y. Krockenberger, M. Noda, H. Yamamoto, D. Manske, L. Alff, and M. Naito, Solid State Commun. **133**, 427 (2005).
[20] Y. Nagata, T. Shioga, T. Taniguchi, T. Uchida, L. Zhang, M. D. Lan, and H. Samata, Phys. Rev. B **65**, 104506 (2002).
[21] E. A. Early, C. C. Almasan, R. F. Jardim, and M. B. Maple, Phys. Rev. B **47**, 433 (1993).
[22] R. Prozorov, D. D. Lawrie, I. Hetel, P. Fournier, and R. W. Giannetta, Phys. Rev. Lett. **93**, 147001 (2004).
[23] J. T. Markert *et al.*, Physica C **158**, 178 (1989).
[24] J. F. Bringley, S. S. Trail, and B. A. Scott, J. Solid State Chem. **87**, 402 (1990).
[25] G. S. Boebinger *et al.*, Phys. Rev. Lett. **77**, 5417 (1996).
[26] D. Sénéchal, P.-L. Lavertu, M.-A. Marois, and A.-M. S. Tremblay, Phys. Rev. Lett. **94**, 156404 (2005).
[27] M. Aichhorn, E. Arrigoni, M. Potthoff, and W. Hanke, Phys. Rev. B **74**, 024508 (2006).
[28] L. Alff, Y. Krockenberger, B. Welter, M. Schonccke, R. Gross, D. Manske, and M. Naito, Nature (London) **422**, 698 (2003).
[29] E. M. Motoyama, G. Yu, I. M. Vishik, O. P. Vajk, P. K. Mang, and M. Greven, Nature (London) **445**, 186 (2007).
[30] S. Karimoto, K. Ueda, M. Naito, and T. Imai, Appl. Phys. Lett. **79**, 2767 (2001).